Comparison of Microwave and Infrared Land Surface Temperature Products Over the NAFE'06 Research Sites

Robert M. Parinussa, Richard A. M. de Jeu, *Member, IEEE*,
Thomas R. H. Holmes, *Member, IEEE*, and Jeffrey P. Walker

***Abstract*—Two different remotely sensed land surface temperature (T_s) products are compared with *in situ* observations from the National Airborne Field Experiment research site in the western part of the Murrumbidgee catchment, Australia. The remotely sensed T_s products are retrieved from the following: 1) Ka-band passive microwave (MW) observations using several of space-based MW radiometers and 2) thermal infrared observations from the Moderate Resolution Imaging Spectroradiometer (MODIS) on two satellite platforms. Both methods show similar accuracy when compared to ground observations, although the dynamic range and mean differ significantly. However, a direct comparison of the two products at the same overpass time reveals a strikingly constant relation, with a standard error of ∼4 K. The results of this study indicate that a merged T_s product of both MODIS and MW observations is feasible and would decrease the amount of data gaps and increase the sampling frequency for this region to 12 observations a day.**

***Index Terms*—Land surface temperature (T_s), microwave (MW) radiometry, National Airborne Field Experiment (NAFE), thermal infrared (TIR).**

I. Introduction

LAND surface temperature (T_s) is defined as the thermodynamic temperature of the uppermost layer of the Earth's surface. It is an important variable in the processes controlling energy, water, and biogeochemical fluxes over the interface between the Earth's surface and the atmosphere. In order to study these processes at the regional to global scale, remote sensing methodologies for measuring T_s must be developed, matured, and widely tested to enable routine measurement of this important variable. For studies at resolutions of 1–100 km^2, it is a huge benefit to have spatially averaged values that remote sensing offers, instead of point measurements that need spatial interpolation. Aside from the ability to monitor large and remote areas, satellites have the important advantage that they can do this consistently over an extended period of time. Commonly used T_s products are derived from thermal infrared (TIR) sensors (e.g., AVHRR, Moderate Resolution Imaging Spectroradiometer (MODIS), or METEOSAT). These TIR-based remote sensing approaches have a spatial resolution of up to 1 km × 1 km, but the temporal continuity is hampered by clouds that block infrared radiation.

Land surface temperature is also a key input variable in several passive microwave (MW)-based global soil moisture retrieval methodologies (see, e.g., [1] and [2]). To benefit from the cloud penetrating properties of passive MWs, the T_s for these retrieval methods should also be independent of clouds. For this reason, there is great interest in methods to derive T_s from passive MW observations [3]–[5]. Within the MW region, vertical polarized Ku-band (18 GHz) and Ka-band (∼37 GHz) observations are best suited for temperature sensing because these bands have a relatively high atmospheric transmissivity [6], combined with a reduced sensitivity to soil surface characteristics. Of these two bands, the Ku-band has the highest atmospheric transmissivity and the highest transmissivity of the vegetation which results in a higher sensitivity to soil surface parameters. For both channels, the vertical polarized observations are best suited for temperature sensing because of its higher emissivity and lower sensitivity to changes in soil moisture at incidence angles of 50°–55°. For these reasons, the vertical polarized Ka-band is deemed the most appropriate choice for single-channel temperature retrievals. In fact, the land parameter retrieval model (LPRM) method [1] is an example of a successful implementation of a linear one sensor Ka-band temperature retrieval [7], [8]. For global soil moisture products, the target accuracy is 0.06 m^3 · m^{-3}; to achieve this at C-band (6–7 GHz) and under bare soil conditions, the accuracy of T_s must be within 4 K. The spatial resolution of measurements at this frequency is typically around 15 km × 10 km, and snow and frozen conditions under wet circumstances prevent the retrieval of T_s from MWs because they result in large differences in dielectric properties. Moreover, rain-bearing clouds or active precipitation with droplets close to the size of the wavelength (8 mm for 37 GHz) will scatter the MW emission [9].

This Ka-band temperature retrieval is recently expanded with the help of a global ground truth network and more strictly related to the skin temperature [10], [11], instead of to the 1-cm

Manuscript received June 4, 2008; revised August 22, 2008. Current version published October 22, 2008. This work was supported in part by the Integrated Project Water and Global Change (WATCH) under Grant EU FP6 and the Australian Research Council (Grant #DP0557543).

R. M. Parinussa, R. A. M. de Jeu, and T. R. H. Holmes are with the Department of Hydrology and Geo-Environmental Sciences, Faculty of Earth and Life Sciences, Vrije Universiteit Amsterdam, 1081 HV Amsterdam, The Netherlands (e-mail: r_parinussa@hotmail.com; richard.de.jeu@falw.vu.nl; thomas.holmes@falw.vu.nl).

J. P. Walker is with the Department of Civil and Environmental Engineering, The University of Melbourne, Melbourne, Vic. 3010, Australia (e-mail: j.walker@unimelb.edu.au).

Color versions of one or more of the figures in this paper are available online at http://ieeexplore.ieee.org.

Digital Object Identifier 10.1109/LGRS.2008.2005738

TABLE I
SPECIFICATIONS OF THE GROUND MEASUREMENT SITES

Parameters	S1	S2	S3
Geographic Location	34.957 S 146.027 E	35.089 S 146.129 E	34.973 S 146.008 E
Sensor type	Ahlborn TIR	Everest TIR	Everest TIR
Soil properties	Bare soil	Irrigated Wheat	Irrigated pasture

NB: In NAFE numbering these sites are indicated as S2, S3, and S4.

soil temperature as was the case in LPRM. Holmes *et al.* [10] showed accurate T_s estimates with Ka-band MW observations for vegetated regions. Based on nine forest field sites, they calculated an average standard error (SE) of 2.2 K. However, they also demonstrated a rapid decrease in accuracy in T_s to above 3 K for semiarid to desert sites.

The main objective of this study is to test the validity of MW T_s in such a semiarid region. For this purpose, both the official remotely sensed MODIS land surface temperature product and T_s ground observations of the National Airborne Field Experiment 2006 (NAFE'06) campaign [12] were compared to satellite-derived MW T_s observations. The NAFE'06 campaign was located in the western part of the Murrumbidgee catchment, Australia. The two satellite-based methods essentially measure the area-weighted average of the temperatures of the various land covers within a specific scene, i.e., a combination of bare soil temperature and vegetation temperature. The satellite-derived T_s will therefore be compared to the ground-based measurements of TIR, which has the same characteristic if installed above the vegetation canopy.

II. MATERIALS AND METHODS

A. Study Area and Ground Measurements

In situ ground measurements of surface temperature were collected as part of the NAFE'06. A subgoal of this experiment was to estimate surface soil temperature from routine remote sensing data at the paddock spatial scales of 100 m × 100 m to 1 km × 1 km [12]. In the Yanco area, TIR sensors were located at three sites, selected based on their land cover that is representative for the region (at paddock scale). At these locations, the land surface temperature and soil temperature at 1-cm depth were measured for the period between October 31, 2006 and November 19, 2006 with a temporal resolution of 20 min. Table I gives a short description of each site. The land surface temperature was measured with TIR instruments with a wavelength range of 8–14 μm. They were installed at 2 m above the ground and calibrated with a water bath before the campaign. The TIR measurements are converted to T_s, assuming an emissivity of 0.95. Although, for natural surfaces, this emissivity might range from 0.9 to 0.99, it can be assumed to be constant over the three-week measurement period. For this study, no corrections are made for possible deviations from the default emissivity because it will not affect the temporal characteristics that are presently investigated. The soil temperature at 1-cm depth was measured with soil thermistors. The accuracies of both the soil thermistor and the TIR instrument are about 0.1 K.

TABLE II
SPECIFICATIONS OF THE KA-BAND MW SENSORS

Parameters	AQUA AMSR-E	DMSP SSM/I (F13)	DMSP SSM/I (F14)	TRMM TMI
Freq. (GHz)	36.5	37	37	37
Polarization	H, V	H, V	H, V	H, V
Inc. angle	55 º	53.1º	53.1º	52.88 º
Footprint. (km)	14 x 8	37 x 28	37 x 28	16 x 10
Swath Width (km)	1445	1394	1394	759
Orbit type	Polar	Polar	Polar	N38º to S38º
Asc. Orbit (UTC)	13:30	17:35	20:21	Variable
Desc. Orbit (UTC)	01:30	05:35	08:21	Variable

Abbreviations are as follows: Aqua-AMSR-E, Advanced Microwave Scanning Radiometer for EOS; DMSP-SSM/I Defense Meteorological Satellite Program Special Sensor Microwave/Imager; TRMM-TMI Tropical Rainfall Measuring Mission Microwave Imager.

B. Passive MW Observations

Ka-band brightness temperatures are currently observed by various satellite platforms (e.g., DMSP, Aqua, TRMM). For four different sensors, the Ka-band data are extracted with the center of pixel nearest to the ground stations. The specifications of the MW sensors are listed in Table II.

The brightness temperatures are converted into T_s ($T_{S,MW}$) according to Holmes *et al.* [10], [11]

$$T_{S,MW} = 1.11 T_{B,Ka} - 15.20 \quad \text{for} \quad T_B > 259.8\,\text{K} \qquad (1)$$

where $T_{B,Ka}$ is the observed Ka-band brightness temperature at vertical polarization in kelvins. This simple linear relation is based on a calibration study with T_s as calculated from long-wave emission measurements. Long-wave emission originates from the top of the target area, and as a consequence, the calibrated T_s represents the area-weighted average of the temperatures of the various land covers. The method is calibrated on nine ground sites in Europe and the U.S., with biome types ranging from semiarid to forests, and a further five are used in the validation study. All these sites are part of the Fluxnet database [13]. The reported SEs for this method at these sites are ∼2.5 and ∼3.5 K for forested sites and for sites with lower vegetation densities (grasslands and croplands), respectively.

C. MODIS

MODIS is a key instrument onboard the Terra and Aqua satellites. Terra's orbit around the Earth is timed so that it passes from north to south across the equator in the morning, while Aqua passes south to north over the equator in the afternoon. Terra MODIS (MOD) and Aqua MODIS (MYD) view the entire Earth's surface every 1 to 2 days, acquiring data in 36 spectral bands of wavelengths (http://modis.gsfc.nasa.gov/about/). The MODIS T_s ($T_{S,MOD}$ and $T_{S,MYD}$) products are produced at 1-km spatial resolution according to the generalized split window technique [14] (version 11A1). The temporal coverage

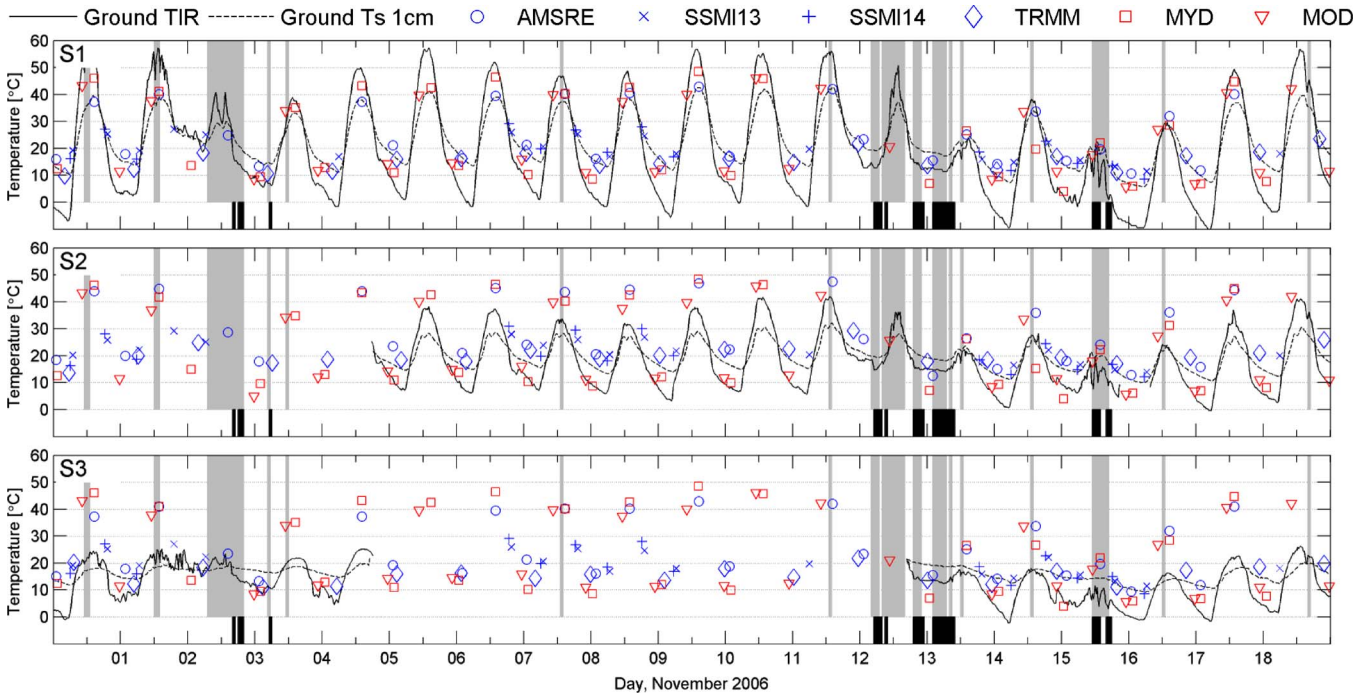

Fig. 1. Time series of (black) TIR ground observations, (blue) MW observations, and (red) downscaled MODIS observations 20 km × 20 km. Gray areas indicate periods with clouds; black areas indicate hours with rainfall.

is affected by the cloud cover at the moment of the satellite overpass.

In this study, two sets of MODIS observations are prepared for each ground station. One set contains the single-pixel (1 km × 1 km) observations over the ground station. The second MODIS data set is downscaled to a 20 km × 20 km box, centered on the ground station, so that the resolution is in better agreement with the MW data.

D. Meteorological Observations

Hourly radiation and precipitation data are collected at the meteorological site of the Bureau of Meteorology of the Australian Government in Wagga (latitude 35.11° S, longitude 145.94° E). As a measure of cloud cover, the ratio between the incoming short-wave radiation and the amount of theoretical (extraterrestrial) short-wave radiation was calculated [15], [16]. This cloud ratio for Wagga is used to flag the time periods with possible clouds at the ground stations, using a threshold of 0.9.

III. Results and Discussion

Fig. 1 shows the time-series comparison of T_s as observed on the three ground stations in the Yanco area and derived from passive MW sensors and the downscaled MODIS data. Hours with precipitation are indicated by the black areas at the bottom, and with clouds are by gray areas. It shows that both MODIS and MW T_s broadly capture the diurnal temperature cycle, but the dynamic range does not compare well with the ground observations. At the bare soil plot S1, the satellite data neatly fall between the TIR and 1-cm T_s as measured at the ground site, with the MODIS data more closely correlated to the TIR temperature and the MW data better correlated with the 1-cm temperature. At the vegetated plots S2 and S3, the temperature range of the remote sensing products is equal to or exceeds the *in situ* infrared temperature, although with an offset on the order of 10 °C. At all sites, the MODIS products have a higher dynamic range than the MW products, which can be explained by a slightly higher penetration depth of the MW products.

The MW temperature appears to be performing well under clouded or rainy conditions. The MODIS product is not expected to perform well under clouded conditions and has therefore been masked for clouded conditions. However, on November 14, at both sites S1 and S2, there appears to be a MODIS temperature anomaly that can likely be attributed to clouds. On this day, $T_{S,MYD}$ is 15 °C colder than the simultaneous MW and station T_s observations, instead of close to or slightly warmer as can be seen at other days. Comparing the averaged MODIS temperature for a box of 20 km × 20 km and the single pixel of 1 km × 1 km for each ground station gives an indication of the heterogeneity and the performance of the MODIS T_s product [Fig. 2(a)–(c)]. The fact that the regression line is close to the 1 : 1 line shows that the single pixel is representative for the wider region. The SE of 1.6 °C–1.8 °C is modest and indicates a low heterogeneity. We conclude that the average MODIS data for the 20 km × 20 km can be used as a downscaled product for comparison with the MW data.

The actual comparison between the MW and MODIS observations is shown in relation to the TIR ground observations. Fig. 2(d)–(f) shows ground data against the averaged MODIS 20 km × 20 km temperature, and Fig. 2(g)–(i) shows ground data against the nearest MW observations. For this comparison, the cloud-free days are selected so that the remote sensing products can be compared in an optimal way. The plots include

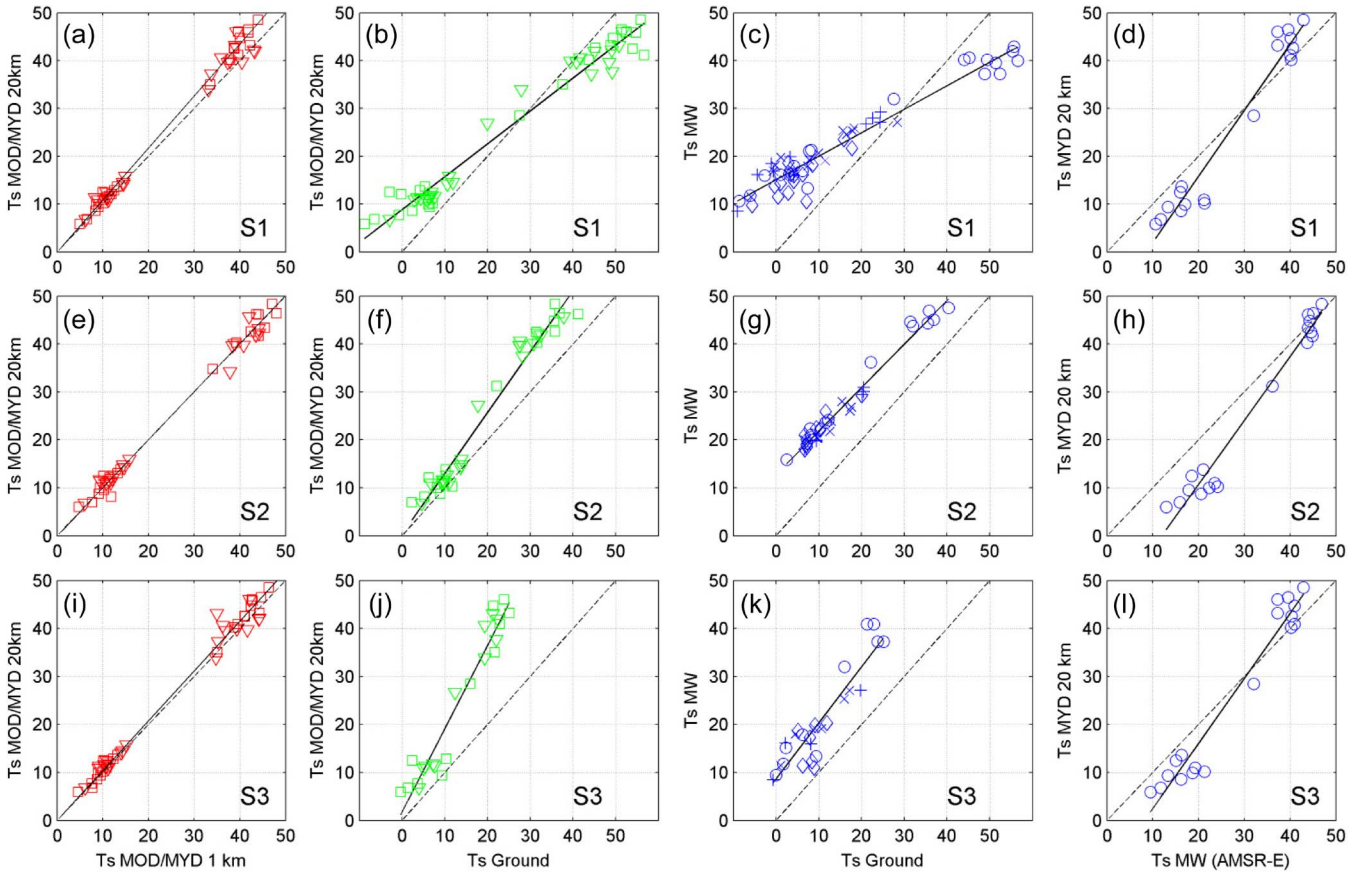

Fig. 2. Scatterplot of temperature observations centered on the three ground stations, from top to bottom and for four different temperature combinations. These data are for the period October 31 to November 18, and unclouded days November 2 and November 12–15.

TABLE III
STATISTICS FOR FIG. 2. SE (IN KELVINS) AND CORRELATION R^2

dT=40K	Ground TIR with:				TMW AMSR with T MYD		T MODIS 1km with T MODIS 20km	
	TMODA		TMW					
	SE	R^2	SE	R^2	SE	R^2	SE	R^2
Whole period from October 31 to November 19								
S1	3.9	0.93	3.3	0.91	4.0	0.94		
S2	4.0	0.93	3.6	0.90	3.8	0.95		
S3	6.5	0.80	5.4	0.74	4.2	0.93		
Unclouded periods (without November 2 and November 12-15)								
S1	2.7	0.97	3.0	0.93	3.9	0.95	1.8	0.99
S2	2.9	0.97	2.1	0.97	3.1	0.97	1.6	0.99
S3	4..1	0.93	4.9	0.84	3.8	0.95	1.8	0.99

data obtained from multiple satellite platforms and show consistency in MODIS observations from MYD (Aqua) and MOD (Terra) and in MW observations from AMSR-E, SSM/I, and TMI. Table III lists the statistics of the scatter plots, together with the slope and the offset of the regression line for the three ground stations. The SE is calculated on the normalized data and then scaled to the data range of MODIS for the investigated ground site. The resulting SE is between 2.7 and 4.1 K for MODIS and between 2.1 and 4.9 K for the MW observations. The correlations (R^2) are high, between 0.93 and 0.97, with one outlier of 0.84 for the MW product at station S3. Overall, the MODIS data have a slightly better performance in terms of SE and, more particularly, in R^2. If the observations under clouded conditions are included, this advantage disappears because the MW product deteriorates less than the MODIS product. Note that in periods with incomplete cloud coverage, the heterogeneity in temperature of the region is increased, which further complicates the point-to-pixel comparison. Part of this detoriation under clouded conditions can be explained by this heterogeneity effect and partly to the increased opacity due to the clouds.

The satellite platform Aqua carries both the MODIS and the AMSR-E sensor and thus offers the opportunity to compare the two temperature products directly for the same observation time. This is shown in Fig. 2(i)–(k) where $T_{\mathrm{S,MYD}}$ is plotted against $T_{\mathrm{S,MW(AMSR-E)}}$. These plots reveal that the strikingly constant relation between the two products and for all sites together is

$$T_{\mathrm{S,MYD}} = 1.32 T_{\mathrm{S,MW(AMSR-E)}} - 11.90 \qquad (2)$$

with temperatures in degree Celsius. Furthermore, the SE is between 3 °C and 4 °C, and R^2 is ∼0.96. These values represent the sum of the true errors of the two individual T_s methods for approximately the same area. Therefore, the true individual errors must be well below 4 °C. It should be noted that part of this error can be attributed to the changing center of the AMSR-E footprint as compared to the fixed 20 km × 20 km box of MODIS.

IV. Conclusion

This investigation in the Yanco area in Australia shows that T_s as retrieved from passive MW observations has a comparable accuracy with the MODIS T_s product. To compare the two products, the MODIS data are downscaled by averaging them over an area of 20 km × 20 km centered on the TIR ground station. Our analysis showed that the heterogeneity of the area is moderate and that the downscaling results only in a minor loss of accuracy for the MODIS product. This downscaled MODIS T_s has comparable accuracy with the MW T_s product, when compared to the ground observations. The SE for both products during cloud-free periods is between 2 and 5 K, with the lowest value for the MW T_s but, overall, a better accuracy and correlation of the MODIS products. This advantage for MODIS disappears when the observations under clouded conditions are included. The MW T_s includes observations from four different satellite platforms. The results show that applying the same linear relationship on MW observations from different sensors to obtain T_s is possible: Different MW sensors show a consistent linear relation.

MODIS observations have a higher spatial resolution (1 km × 1 km) than MW observations. On the other hand, MW observations have a higher temporal resolution (up to five times a day) than MODIS observations (1–2 observations a day). Passive MW T_s observations are much less sensitive to clouds than MODIS T_s observations, which results in fewer gaps in the data. These different characteristics and limitations make the two products complimentary.

A comparison between two sensors onboard the Aqua satellite reveals a strikingly constant relationship between the MODIS and AMSR-E T_s products with an SE of ∼4 °C and R^2 of ∼0.93. These results indicate that merging of the two data sets is feasible for the study area. Further research is necessary to test the stability and temporal consistency of such a merging of MODIS and MW temperature products. Further improvements in the MW temperature products are expected when a global multichannel algorithm becomes available.

Acknowledgment

The authors would like to thank the 2006 National Airborne Field Campaign research team for providing the field data.

References

[1] M. Owe, R. A. M. De Jeu, and T. R. H. Holmes, "Multi-sensor historical climatology of satellite derived global land surface moisture," *J. Geophys. Res.*, vol. 82, no. 20, pp. 3108–3118, Jan. 2008.

[2] E. G. Njoku, T. J. Jackson, V. Lakhsmi, T. K. Chan, and S. V. Nghiem, "Soil moisture retrieval from AMSR-E," *IEEE Trans. Geosci. Remote Sens.*, vol. 41, no. 2, pp. 215–229, Feb. 2003.

[3] R. A. M. De Jeu and M. Owe, "Further validation of a new methodology for surface moisture and vegetation optical depth retrieval," *Int. J. Remote Sens.*, vol. 24, no. 22, pp. 4559–4578, 2003.

[4] M. Fily, A. Royer, K. Goïta, and C. Prigent, "A simple retrieval method for land surface temperature and fraction of water surface determination from satellite microwave brightness temperatures in sub-arctic areas," *Remote Sens. Environ.*, vol. 85, pp. 328–338, 2003.

[5] M. Owe and A. A. Van De Griend, "On the relationship between thermodynamic surface temperature and high-frequency (37 GHz) vertically polarized brightness temperature under semi-arid conditions," *Int. J. Remote Sens.*, vol. 22, no. 17, pp. 3521–3532, 2001.

[6] R. N. Colwell, D. S. Simonett, and F. T. Ulaby, *Manual of Remote Sensing*, 2nd ed, vol. 2. Hoboken, NJ: Wiley, 1983, pp. 1233–2440.

[7] W. Wagner, V. Naeimi, K. Scipal, R. de Jeu, and J. Martinez Fernandez, "Soil moisture from operational meteorological satellites," *Hydrogeol. J.*, vol. 15, no. 1, pp. 121–131, Feb. 2007.

[8] C. S. Draper, J. P. Walker, P. J. Steinle, R. A. M. de Jeu, and T. R. H. Holmes, "Remotely sensed soil moisture over Australia from AMSR-E," in *Proc. MODSIM*, Christchurch, New Zealand, 2007.

[9] F. T. Ulaby, R. K. Moore, and A. K. Fung, *Microwave Remote Sensing: Active and Passive*, vol. III. Norwood, MA: Artech House, 1986.

[10] T. R. H. Holmes, R. A. M. de Jeu, M. Owe, and A. J. Dolman, *Land Surface Temperature From Ka-Band (37 GHz) Passive Microwave Observations*, 2008. In review.

[11] T. R. H. Holmes, "The radiative temperature of the Earth at microwave frequencies," "Ph.D. dissertation," VU Univ. Amsterdam, Amsterdam, The Netherlands, 2008.

[12] O. Merlin, J. P. Walker, J. D. Kalma, E. J. Kim, J. Hacker, R. Panciera, R. Young, G. Summerell, J. Hornbuckle, M. Hafeez, and T. Jackson, "The NAFE'06 data set: Towards soil moisture retrieval at intermediate resolution," *Adv. Water Res.*, 2008. DOI:10.1016/j.advwatres.2008.01.018.

[13] D. Baldocchi, E. Falge, L. Gu, R. Olson *et al.*, "FLUXNET: A new tool to study the temporal and spatial variability of ecosystem-scale carbon dioxide, water vapor, and energy flux densities," *Bull. Amer. Meteorol. Soc.*, vol. 82, no. 11, pp. 2415–2434, 2001.

[14] Z. Wan and J. Dozier, "A generalized split-window algorithm for retrieving land-surface temperature from space," *IEEE Trans. Geosci. Remote. Sens.*, vol. 34, no. 4, pp. 892–905, Jul. 1996.

[15] W. Brutsaert, *Hydrology: An Introduction*. Cambridge, U.K.: Cambridge Univ. Press, 2005.

[16] M. Owe, "The utility of climatic station data in making hourly potential evapotranspiration estimates for remote sensing studies," *J. Hydrol.*, vol. 107, no. 1–4, pp. 99–111, May 1989.